# Aerodynamic Heating in Missile-Fin Interaction Region

Devon Fano,[1] Jonathan Poggie,[2] and Gregory Blaisdell[3]
*Purdue University, West Lafayette, IN 47907-2045, USA*

**Shock wave boundary layer interactions often produce large rates of heating on flight vehicles. This study presents results of a RANS computational investigation to compute the surface heating, as well as other quantities, in the gap region of an ogive-missile and connected fin configuration in Mach 6 flow. The boundary layer on the missile surface enters the gap region and interacts with the boundary layer on the fin underside, the shock produced by the fin tip, and the cylinder connecting the fin to the missile. The grid generation techniques utilized allow all grids to be structured. Wind tunnel experiments found the largest heating rates just upstream of the cylinder. These simulations duplicate this finding as well as other aspects of the flow observed in wind tunnel experiments.**

## Nomenclature

| | | |
|---|---|---|
| $C_f$ | = | skin friction coefficient |
| $h$ | = | gap height between missile surface and fin bottom surface |
| $H$ | = | heat transfer coefficient |
| M.S. | = | missile station |
| $q$ | = | heat flux |
| X/D | = | distance upstream of cylinder surface divided by cylinder diameter |
| $Z$ | = | height above missile surface |
| $\alpha$ | = | angle of attack of missile |
| $\Delta s$ | = | first grid cell spacing off of a surface |
| $\phi$ | = | roll angle of missile |

## I. Introduction

Three-dimensional flow interactions are important to understand for design applications, but difficult to simulate. The flow interactions created by fin/body junctions on high-speed vehicles are especially significant because it is common for surface heating rates to be very high in these regions. Studies have investigated excessive heating in gaps between tiles on the Space Shuttle, and one study by Petley and Smith [1] showed that heating can be excessive enough to cause, "visible discoloration and charring of the filler bar and strain isolator pad (SIP) used in the attachment of tiles to the aluminum substrate." Dolling [2] notes that maximum surface heating in high Mach number shock boundary layer interactions has been well established to reach rates 1 to 2 orders of magnitude above that of the surface underneath the incoming boundary layer.

There have not been many high-fidelity simulations published in the open literature investigating gap regions between flight vehicles and control surfaces. Accurately predicting the value of peak heating has remained elusive, and numerical results are sensitive to the choice of turbulence model. Dolling [2] notes that RANS solvers often predict higher heat transfer rates than those found by experiments. Many studies have correlated the locations of maximum surface pressure and maximum surface heating. One experimental shock boundary layer study by Law [3] found a correlation for location of maximum pressure and maximum heat transfer, but insufficient data were available to correlate magnitudes.

[1] Graduate Student, School of Aeronautics and Astronautics.
[2] Associate Professor, School of Aeronautics and Astronautics, AIAA Associate Fellow.
[3] Professor, School of Aeronautics and Astronautics, AIAA Associate Fellow.

Neumann and Hayes [4] conducted an experimental investigation that involved several Mach 6 wind tunnel tests of an ogive-cylinder with mounted fin-shaped control surfaces. Fins were either sealed to the body or connected via a cylinder, also referred to as a 'torque tube,' creating a gap. The portion of their experiments that is simulated in this study involves a fin with a 15° wedge and a 60° sweep connected to a missile body via a 0.625 inch (1.59 cm) diameter cylinder. The gap height, $h$, varies from 0.2 inches to 0.5 inches. A depiction of this missile-fin configuration is shown in Fig. 1.

Neumann and Hayes studied the effects of $\alpha$, $\phi$, and $h$ on missile surface heating. Using thermocouples, they found heating in the gap region downstream of the cylinder to be very similar to measurements from the interaction region of the sealed fin experiments. The maximum heat transfer coefficient, $H$, downstream of the cylinder occurred at the largest $\alpha$ tested, 12°, the largest $\phi$ tested, 90°, and the smallest $h$ tested, 0.1 inches. This $H$ value is 5 times larger than values measured on the clean-missile surface absent of a fin or cylinder. Upstream of the cylinder in the gap region, $H$ peaked at 17 times the clean-missile levels. This peak occurred at the largest $h$ reported, 0.4 inches, when $\alpha = 8°$ and $\phi = 90°$. The gap region upstream of the cylinder is the focus of this paper because it has the highest rates of heating.

Neumann and Hayes also identified, via oil flow, two possible separation patterns for the flow upstream of the cylinder. For relatively small $h$, surface heating would increase with $h$ and the separation pattern was labeled as Type I. Type I separation was characterized by a continuous oil accumulation line outlining the leading edge of the vortex surrounding the cylinder. As $h$ increased, a critical gap height would be reached and the separation pattern would switch to Type II. Type II separation was characterized by a discontinuous oil accumulation line tracing the leading edge of the vortex that intersected the separation closest to the cylinder. A noticeable drop in surface heating accompanied this switch. Maximum surface heating would then continue to rise with $h$ as it did with the Type I separation pattern. This critical $h$ could not be precisely correlated but it depended on $\alpha$ and $\phi$ and fell between 0.2 and 0.4 inches. A notable observation was that at $\alpha = 0°$, a switch from the Type I pattern to the Type II pattern would not occur in the range of $h$ tested. For all simulations in this paper, $\alpha = 0°$ and $\phi = 0°$.

## II. Methodology

The air freestream flow conditions were chosen to match those used in the wind tunnel experiments of Neumann and Hayes [4] and are presented in Table 1.

**Table 1 Freestream flow conditions.**

| | |
|---|---|
| Mach Number ($M_\infty$) | 5.95 |
| Freestream Velocity ($u_\infty$) | 901.1 m/s |
| Static Pressure ($P_\infty$) | 1149 Pa |
| Static Temperature ($T_\infty$) | 57.06 K |
| Density ($\rho_\infty$) | 0.0702 kg/m$^3$ |
| Viscosity ($\mu_\infty$) | $3.753 \times 10^{-6}$ kg/m/s |
| Reynolds Number ($Re_\infty$) | $1.684 \times 10^7$ |
| Length Scale (L) | 1 m |

In Neumann and Hayes's experiments, the missile was injected into the wind tunnel when thermocouples measured less than 85°F. The simulations in this study utilize isothermal wall conditions for both the missile and fin surfaces at 300 K (80°F). The open source CFD code SU2 [5] was used to perform all numerical simulations. It is a finite volume, unstructured solver that employs a median-dual vertex-based scheme. It's Reynolds-averaged Navier-Stokes solver (RANS) was utilized to simulate the viscous, compressible flow involved in this investigation. There are multiple options for the numerical methods used by SU2. A list of selected SU2 configuration settings utilized in all simulations in this study is shown in Table 2 in the Appendix.

A depiction of the missile-fin configuration when $h = 0.5$ inches is shown in Fig. 1. The total length of the missile is 50 inches (1.27 m) and its base diameter is 8.5 inches (0.216 m). The symbol for Missile Station, M.S., is measured in inches and represents distance from the missile tip along the center missile axis. For reference, the gap region begins at the fin tip at M.S. 42, the center of the cylinder is at M.S. 46.25, and the end of the fin region is at M.S. 48. A missile tip radius of 50 microns was assumed during the creation of all grids.

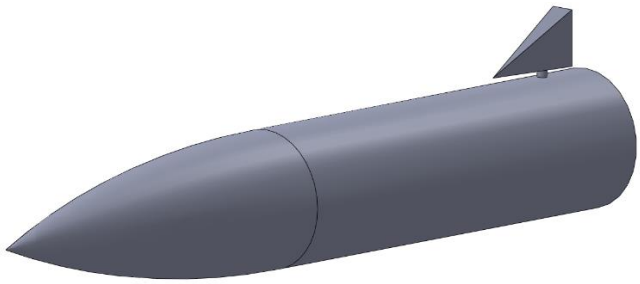

**Fig. 1 Missile-fin configuration.**

Clean-missile simulations were performed prior to missile-fin simulations. The clean-missile configuration involves the bare missile surface absent of a cylinder or fin. These simulations were used to establish baseline boundary layer and surface heating data for comparison to the missile-fin results. Also, Neumann and Hayes performed tests on the clean-missile configuration, so results are compared to their findings. A coarse grid and a fine grid were created to simulate the clean-missile configuration. Although the flow is axisymmetric, 3D grids were utilized to be consistent with the 3D grids used to simulate the missile-fin configuration. Both clean-missile grids were created from a 90° rotation of the domain above the missile profile, which results in two symmetry planes. Figure 2 shows the coarse grid, which contains 165 points across the missile surface in the x-direction, 200 points in the y-direction, 21 points in the circumferential direction, and 693,000 points total. The fine grid contains 423 points across the missile surface in the x-direction, 400 points in the y-direction, 21 points in the circumferential direction, and 3,553,200 points total. All grids utilized in this study were created using the commercial grid generation program, Pointwise [6].

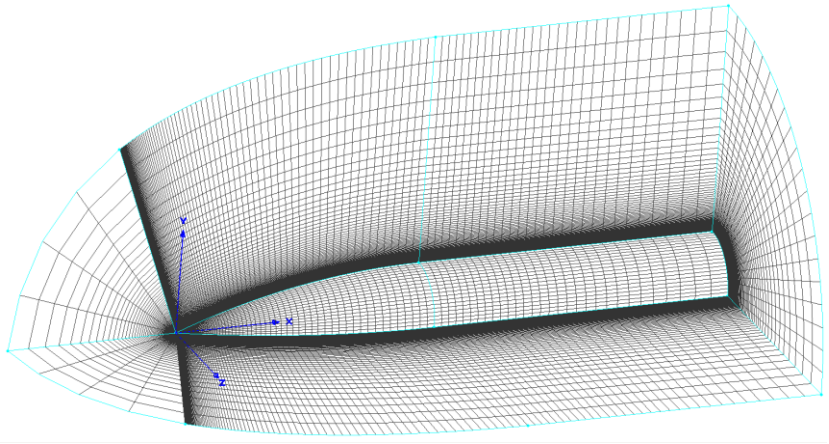

**Fig. 2 Coarse clean-missile grid.**

In Neumann and Hayes's experiments, a 0.75-inch wide band of grit was placed 4 inches from the missile tip to ensure that a turbulent boundary layer existed over the entire missile surface. The Spalart-Allmaras [7] turbulence model was utilized in all simulations in this investigation to approximate the effects of that grit strip. Also, the wall normal grid spacing, $\Delta s$, off of the missile surface was chosen to achieve $y^+ = 1$ almost everywhere. The definition of $y^+$ can be rearranged to state that

$$y^+ = \frac{\rho\, u\, \Delta s}{\mu} \sqrt{\frac{C_f}{2}}. \tag{1}$$

By approximating using freestream values, Eq. (1) can be rearranged to show that

$$\Delta s(y^+ = 1) = \frac{L}{Re_\infty} \sqrt{\frac{2}{C_f}}. \tag{2}$$

By approximating using the skin friction coefficient relation [8], which ignores Mach number effects, that

$$C_f = \frac{0.026}{Re_\infty^{\frac{1}{7}}}, \tag{3}$$

$\Delta s$ can be calculated as a function of $Re_\infty$. Using the $Re_\infty$ from this investigation, $\Delta s = 1.7 \times 10^{-6}$ m. All grids employ this $\Delta s$ off of the missile surface. After solutions converged, $y^+$ was checked on the missile surface for all simulations. It was calculated that $y^+ < 0.5$ held everywhere, including the gap region, except very near the missile tip.

The grids used to simulate the missile-fin configuration contain 20 to 30 million points each. Decisions regarding grid point counts were made to maximize the number of points in the gap region upstream of the cylinder given computational resources. Due to the structured nature of the grids, increasing grid density in the gap region also increased grid density in other regions. This propagation of grid density is one drawback of structured grids. Exclusively structured grids were chosen for this study, however, because they often result in more accurate solutions than unstructured grids with comparable cell counts [9]. A 3D structured grid is defined as containing only hexahedra. Due to the complex geometry of the missile-fin configuration, it is not possible to design a single structured grid that models the whole topology. Therefore, a multiblock structured grid design was used. The overall configuration was divided into sub-domains that were each modeled with a single structured block grid. These blocks connect via shared faces and cover the entire configuration. Figures 3 and 4 identify the 22 blocks used in the missile-fin grids. Figure 5 shows the surface meshes on the fin underside, cylinder, and missile in the gap region. The fin underside mesh was projected onto the missile surface using the projection feature in Pointwise. Most of this surface mesh was projected using a closest-point approach, which results in grid orthogonality on the missile surface. However, the cylinder profile was projected using a linear approach to accurately model the cylinder used in Neumann and Hayes's experiments.

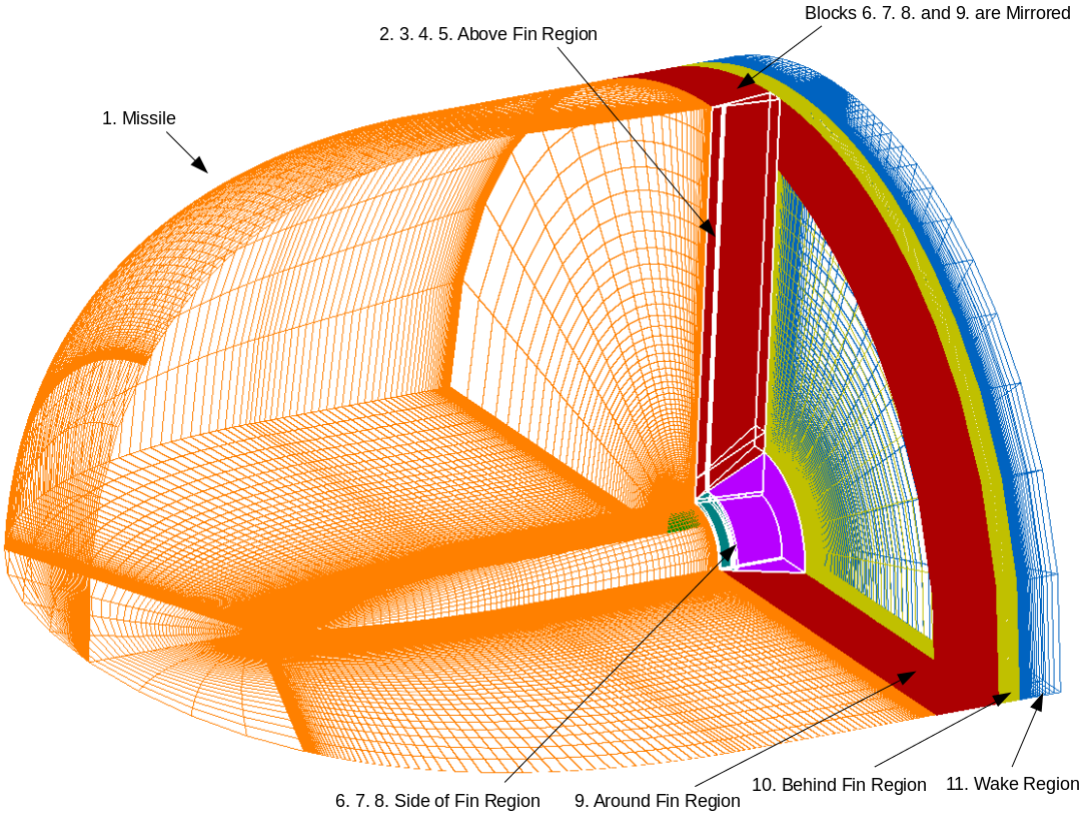


**Fig. 3 Missile-fin grid ($h = 0.3$ inches).**

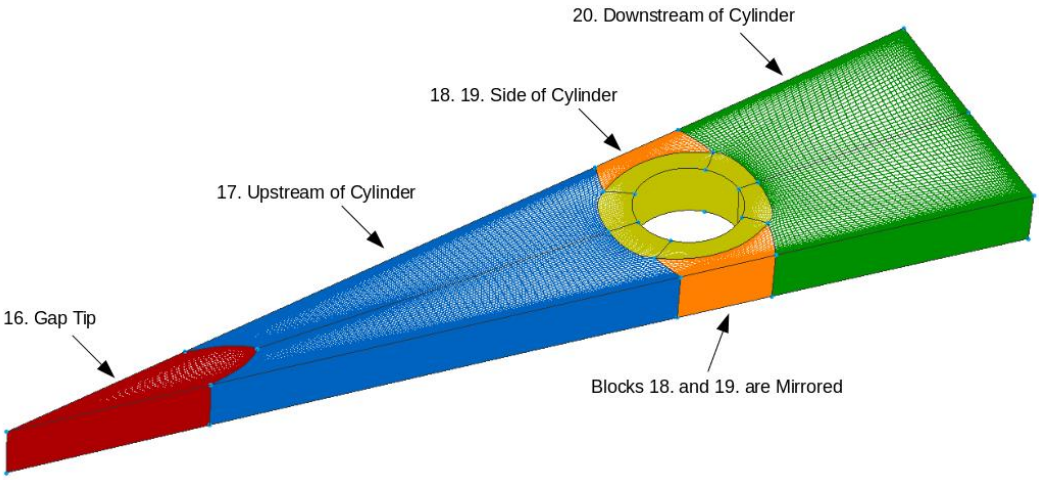


**Fig. 4 Gap region grid ($h = 0.3$ inches).**

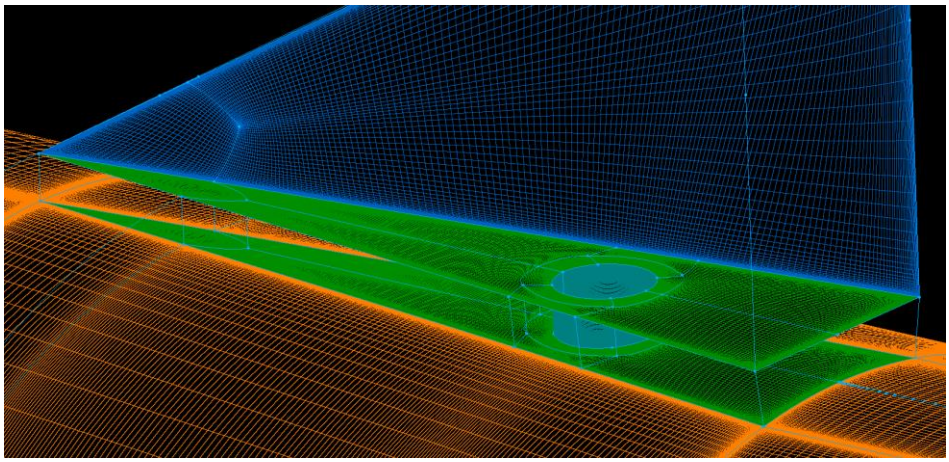

**Fig. 5 Gap region surface meshes ($h = 0.3$ inches).**

As shown in Fig. 3, grid density decreases far from the fin region. It is assumed that the levels of resolution of the surrounding freestream, missile shock, and wake regions do not significantly influence the gap region upstream of the cylinder. The seven blocks in the gap region contain about 4 million points. Connecting lines across the gap contain about 200 points. The blocks that make up the region around, above, and on the side of the fin contain about 10 million points. Due to the flow's high Reynolds number, a very small $\Delta s$ is necessary to achieve $y^+ < 1$ on the missile surface and fin surface. Achieving $y^+ < 1$ on the fin surface is the primary inflator of the overall point count. It is also is the reason why the x-direction grid lines on the missile surface curve toward the tip of the fin region. A symmetry plane can be employed to avoid resolving the lower half of the missile. Defining the origin of the coordinate system to be the missile tip, the x-axis to be parallel with the freestream, and the y-axis to be parallel with the axis of the cylinder when $\alpha = 0°$ and $\phi = 0°$, the symmetry plane is located at y = 0. Although these missile-fin grids do not utilize it, a z=0 symmetry plane is possible and recommended.

The triangular faces of the fin required special consideration. A curved line can be used to separate a triangle into a pair of 4-sided regions. All four triangular fin faces were separated near the tip and the result of this process on the side fin face is shown in Fig. 6. Extensive application of the Steger-Sorenson boundary control function [10], via Pointwise's grid solving tool, ensured that grid smoothness was maintained at the grid separation line. It also enforced specified $\Delta s$ values and orthogonality on edges.

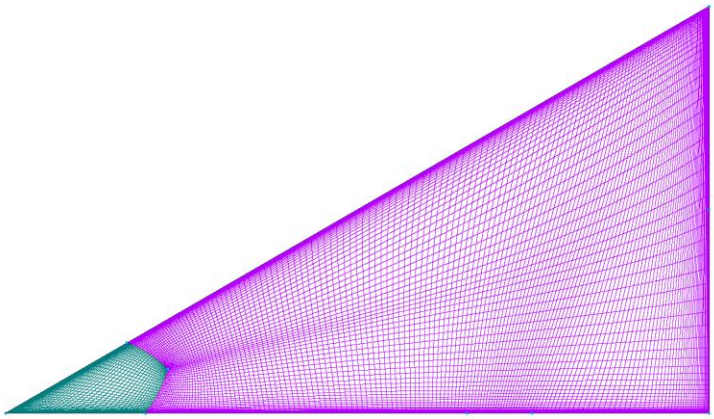

**Fig. 6 Side fin face surface mesh.**

## III. Results

### A. Clean-Missile Boundary Layer

A Mach contour plot of the converged clean-missile simulation is shown in Fig. 7. The methodology used to determine convergence for all simulations is discussed in the Appendix. All Mach contour plots were created using the commercial plotting program, Tecplot [11]. Neumann and Hayes report measurements of the clean-missile boundary layer, when $\alpha = 0°$ and $\phi = 0°$, at M.S. 42. The value $P_T/P_{0_2}$ is plotted in 0.1 inch intervals from $Z = 0.1$ inches to $Z = 1.0$ inch above the missile surface. The symbol, $Z$, refers to distance above the missile surface and is different than z in Fig. 2. According to Neumann and Hayes's List of Symbols, $P_T$ is "Pressure - Total (Pitot Probe) Value" and $P_{0_2}$ is "Pressure - Stagnation Value – Local Value Downstream of Normal Shock". The following assumptions make simulated results show agreement with Neumann and Hayes's measurements. $P_T$ is the $P_{Pitot}$ at a given point in the boundary layer and $P_{0_2}$ is the $P_{Pitot}$ in the freestream. The $P_{Pitot}$ of a point in the flow is the stagnation pressure downstream of a hypothetical normal shock. When Neumann and Hayes measured pressure in the boundary layer, using a Pitot rake, there were normal shocks upstream of the Pitot tubes. Given $P$ and $M$ outputs from SU2, $P_{Pitot}$ can be calculated by using isentropic flow and normal shock relations. This calculation is sometimes referred to as the *Rayleigh Pitot formula* (see Appendix for the Python [12] function written to perform this calculation). Figure 8 shows the simulated clean-missile boundary layer compared to Neumann and Hayes's measurements at M.S. 42. All plots were created using the Python libraries Numpy [13] and Matplotlib [14]. The boundary layer thickness is defined by Neumann and Hayes to be the point on the plot where a knee occurs. Simulated results show excellent agreement with measured data for knee location, which is about 0.6 inches above the missile surface.

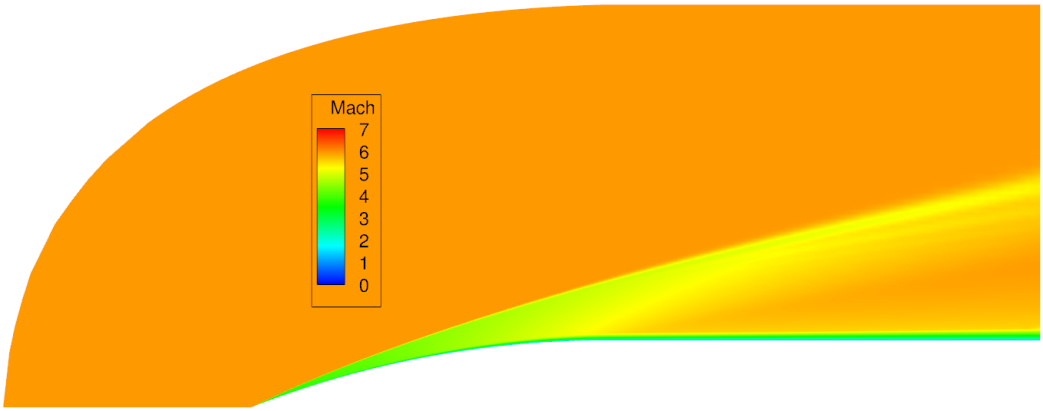


**Fig. 7 Mach contour plot of clean-missile simulation (fine grid).**

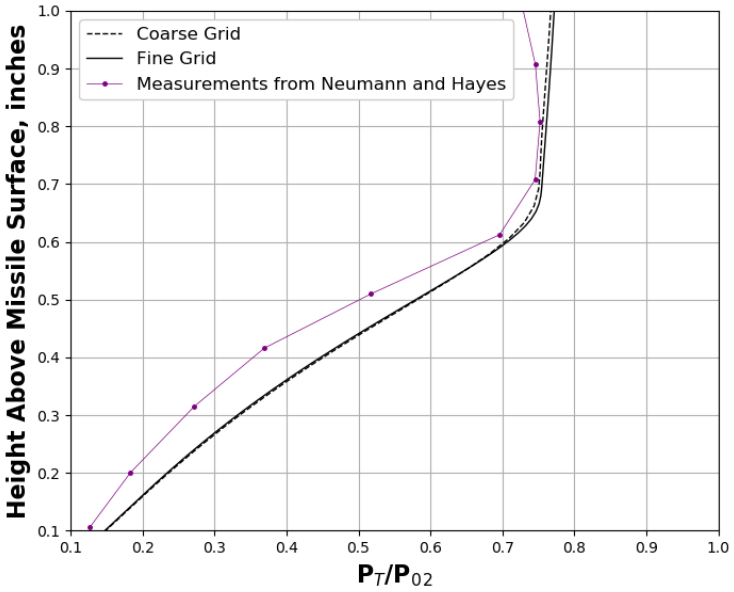


**Fig. 8 Simulated clean-missile boundary layer at M.S. 42 compared to measurements from Neumann and Hayes [4, their Figure 4.27].**

### B. Clean-Missile Surface Heating

Regarding surface heating, it is better to analyze $H$ rather than $q$ because $H$ is normalized by surface temperature. However, SU2 only outputs $q$, and in units of W/m$^2$. The units of heat transfer coefficient used by Neumann and Hayes are BTU/ft$^2$/s/R. It is possible to convert between the two units as follows:

$$\left(1\frac{BTU}{ft^2\ s\ R}\right)\left(10.7639\frac{ft^2}{m^2}\right)\left(1055.06\frac{J}{BTU}\right)\left(1.8\frac{R}{K}\right) = 20442\frac{W}{m^2\ K}. \tag{4}$$

Also, the definition of $H$ used by Neumann and Hayes is

$$H = \frac{q}{(T_{\infty_0}\ r) - T_{wall}}, \tag{5}$$

where $T_{\infty_0}$ is the freestream stagnation temperature, $r$ is the recovery factor, and $T_{wall}$ is the surface temperature at the point where $H$ is being calculated. The value $T_0\ r$ is meant to represent $T_{Recovery}$, which is the adiabatic surface temperature after thermal equilibrium with the boundary layer is reached. The temperature, $T_{Recovery}$, could not be measured by Neumann and Hayes due to issues with thermocouple durability, so values of $r$ were approximated by extrapolating data. At $\alpha = 0°$, Neumann and Hayes report $H$ on the clean-missile surface only at M.S. 35. Based on the plot labeling, $r = 0.9$. Their data points fall between 30% and 50% of the distance on a log scale between $1 \times 10^{-3}$ BTU/ft$^2$/s/R and $2 \times 10^{-3}$ BTU/ft$^2$/s/R. These values are $1.23 \times 10^{-3}$ BTU/ft$^2$/s/R and $1.41 \times 10^{-3}$ BTU/ft$^2$/s/R. Simulated results of the $H$ distribution compared to Neumann and Hayes's data are shown in Fig. 9. At M.S. 35, clean-missile simulations resulted in $H = 1.32 \times 10^{-3}$ BTU/ft$^2$/s/R. This result, which falls exactly center of Neumann and Hayes's range of measurements, indicates that excellent agreement between measured and simulated heat transfer coefficients on a clean-missile surface is possible. It also provides evidence that the Spalart-Allmaras turbulence model is a good choice for surface heating simulations.

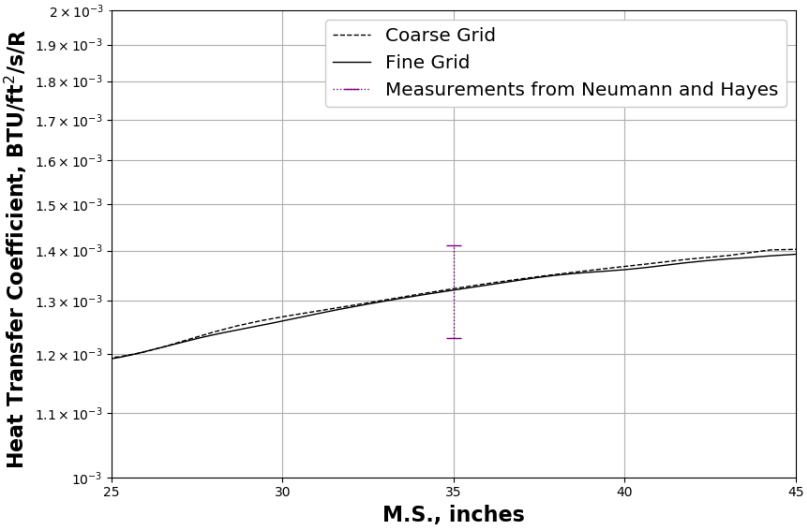


**Fig. 9 Simulated clean-missile heat transfer coefficient compared to measurements from Neumann and Hayes [4, their Figure 4.11].**

### C. Missile-Fin Skin Friction and Surface Pressure

Four gap heights were simulated for the missile-fin configuration: $h = 0.2$, 0.3, 0.4, and 0.5 inches. Figure 10a shows a Mach contour plot, at the z=0 slice plane, from each $h$ simulation. A simulation for $h = 0.1$ inches was attempted but did not achieve convergence. Smaller gap heights were harder to simulate than larger gap heights. Identifiable flow features from these plots include the missile boundary layer upstream of the fin, an oblique shock on the top fin surface, a high-velocity expansion region downstream of the top corner of the fin, and wake regions behind the fin and missile. The $h = 0.2$ inches simulation appears to have numerical errors above the top oblique shock, but it is assumed that these errors do not influence the results in the gap region. Directly upstream of the cylinder, the Mach contour plot exhibits a lambda-shape when $h = 0.4$ inches and $h = 0.5$ inches. Streamlines indicate flow separation and a recirculation region at this location for all four $h$ simulated. These streamlines are displayed in Fig. 10b. Also, the skin friction coefficient outputted by SU2, $C_{f_x}$, is plotted in the gap region upstream of the cylinder on the missile surface centerline in Fig. 11. Separation occurs where $C_{f_x} = 0$. The location of separation for all $h$ simulated is near X/D = 1.75. The ratio, X/D, refers to distance upstream of the cylinder surface in units of cylinder diameters. For reference, the fin tip is at X/D = 6.3.

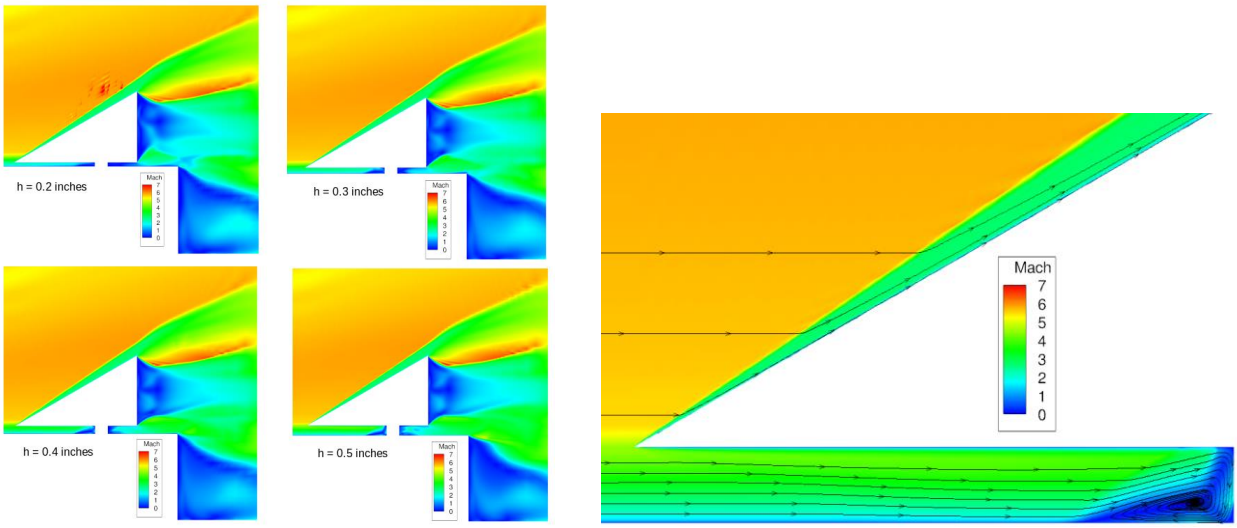


a) Fin region for all $h$ simulated. b) Fin region with streamlines ($h = 0.5$ inches).

**Fig. 10 Mach contour plots from missile-fin simulations.**

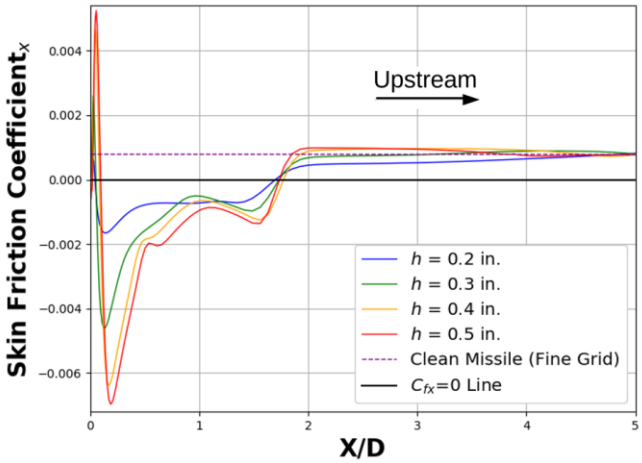


**Fig. 11 Simulated $C_{f_x}$ upstream of cylinder surface.**

Surface pressure was not measured by Neumann and Hayes in the gap region, so simulated results cannot be compared to their experiments. Figure 12 plots pressure on the missile surface centerline in the gap region upstream of the cylinder for all $h$ simulated. In all cases, maximum pressure occurs very close to the cylinder. As highlighted in the magnified box, the influence of the fin and cylinder on surface pressure extends farther from the cylinder at smaller $h$. Surface pressure approaches the clean-missile value closer to the cylinder for larger $h$. This effect may be caused by the fin tip shock having to travel further downstream before meeting the missile surface at larger $h$.

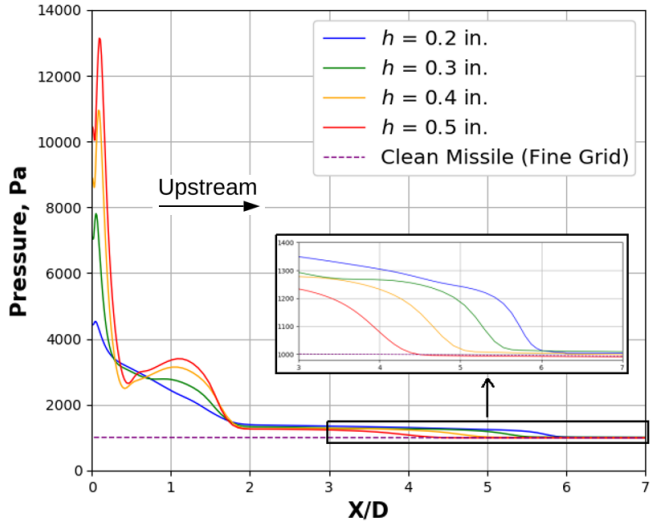


**Fig. 12 Simulated missile surface pressure upstream of cylinder surface.**

### D. Missile-Fin Surface Heating

Simulated $H$ distributions on the missile surface upstream of the cylinder are compared to Neumann and Hayes's data in Fig. 13. For $\alpha = 0°$ and $\phi = 0°$, Neumann and Hayes only reported data for $h = 0.3$ inches. Notable details from Neumann and Hayes's data are that the maximum $H$ occurs very close to the cylinder, $H$ generally increases with $h$, and $H$ tends to decrease moving away from the cylinder. These details are also true for their tests involving nonzero $\alpha$ and $\phi$ and they are true for simulated results. As found by Law [3], and others, the locations of maximum surface pressure and maximum $H$ are very similar for simulated results. In Neumann and Hayes's $\alpha = 8°$ plot, which is not shown here, $H$ decreases between $h = 0.3$ inches and $h = 0.4$ inches due to a flow separation pattern change that does not occur at $\alpha = 0°$. Simulations do not indicate this decrease, as expected. Also, Neumann and Hayes noted that, "the interaction was found to extend about two diameters upstream of the torque tube...," implying that $H$ approaches clean-missile levels upstream of X/D = 2. Simulations did result in this situation. All $H$ distributions approach the level shown in Fig. 9, which is on the order of $10^{-3}$ BTU/ft$^2$/s/R, upstream of X/D = 2. Neumann and

Hayes's data, however, involve $H$ approaching $10^{-4}$ BTU/ft$^2$/s/R upstream of X/D=2. No realistic recovery factor can cause this discrepancy, so its source is unknown. Simulated results are scaled in Fig. 13 so that the $h = 0.3$ inches results coincided with the most upstream point from Neumann and Hayes's data.

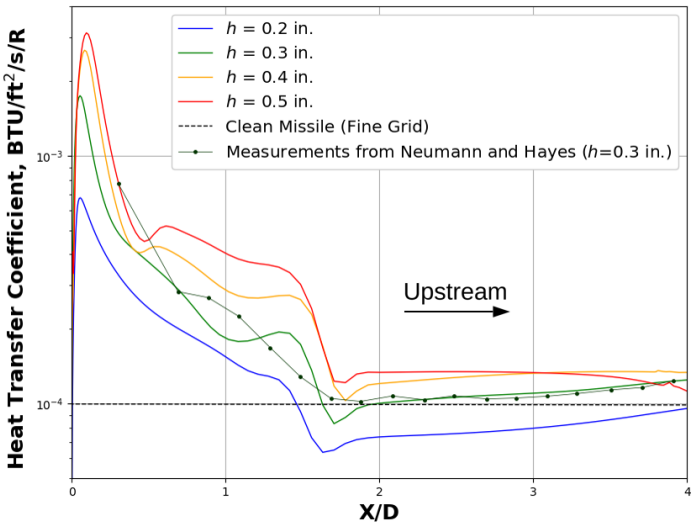


**Fig. 13 Simulated missile-fin heat transfer coefficient (scaled) upstream of the cylinder surface compared to measurements from Neumann and Hayes [4, their Figure 6.10].**

Neumann and Hayes report peak heating in the gap region upstream of the cylinder, for $\alpha = 0°$ and $\phi = 0°$, at $h = 0.1$, 0.2, 0.3, and 0.4 inches. The maximum $H$ occurred at the closest thermocouple to the cylinder surface, which is at X/D = 0.3, for all reported tests. The values are normalized by $H_U$, or $H_{clean}$, which is the $H$ value on the clean-missile surface. Figure 14 compares Neumann and Hayes's $H/H_{clean}$ to the scaled simulation results at X/D = 0.3. Neumann and Hayes did not specify $H_{clean}$, but it can be assumed to be about $1 \times 10^{-4}$ BTU/ft$^2$/s/R. For $h = 0.3$ inches, $H_{peak}/H_{clean}$~8 and $H_{peak}$~$8 \times 10^{-4}$ BTU/ft$^2$/s/R. Therefore, $H_{clean}$ was assumed to be $1 \times 10^{-4}$ BTU/ft$^2$/s/R during normalization of the scaled simulation results. Their statement, "...the peak heating location being no more than 0.3 diameters upstream," possibly indicates that Neumann and Hayes thought it possible that peak heating can occur closer to the cylinder than X/D = 0.3. Simulated results show this occurrence, with peak $H$ occurring between X/D = 0.05 and X/D = 0.1 for all $h$ simulated. Figure 15 plots the maximum simulated $H$ values. Neumann and Hayes's measured $H/H_{clean}$ values at X/D = 0.3 fall between the simulated values at X/D = 0.3 and the peak simulated values.

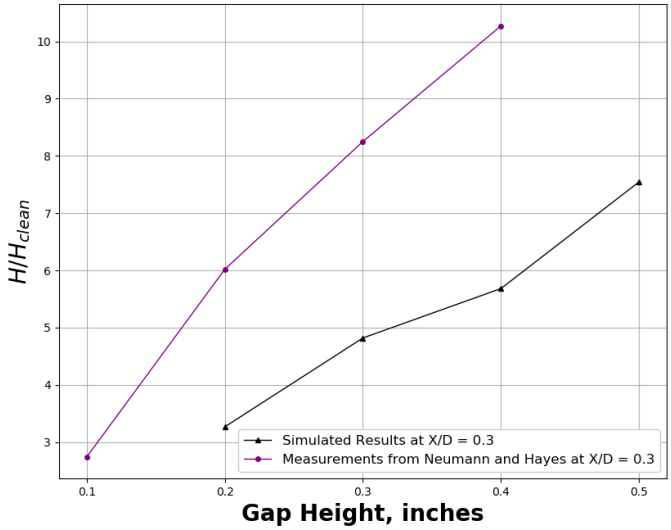


**Fig. 14 Simulated heat transfer coefficient divided by clean-missile heat transfer coefficient at X/D = 0.3. Compared to measurements by Neumann and Hayes [4, their Figure 6.11].**

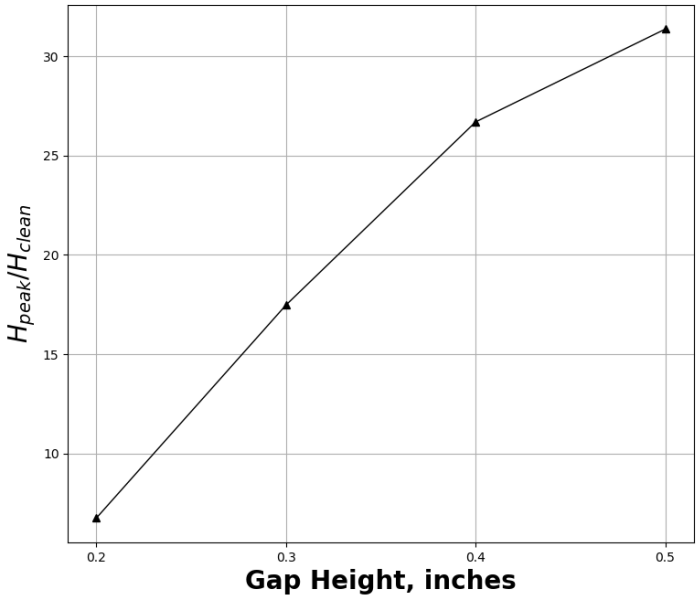


**Fig. 15 Simulated maximum heat transfer coefficient upstream of the cylinder surface in the gap region divided by clean-missile heat transfer coefficient.**

## IV. Conclusion

Simulations predict large rates of heating on the missile surface close to the upstream side of the cylinder. Neumann and Hayes came to the same conclusion based on their wind tunnel tests. Simulated heat transfer coefficients reach a maximum level, which is much higher than Neumann and Hayes's maximum level, closer to the cylinder surface than the closest thermocouple in the wind tunnel tests. The design point for surface heating, stated by Neumann and Hayes to be within 0.3 cylinder diameters upstream of the cylinder surface, is predicted by these simulations to be closer to 0.1 cylinder diameters. Future simulations will involve varying $\alpha$ and $\phi$ to generate more results to compare to experimental data.

## Appendix

**Table 2 SU2 configuration settings.**

| | |
|---|---|
| NUM_METHOD_GRAD | GREEN_GAUSS |
| LINEAR_SOLVER | FGMRES |
| CONV_NUM_METHOD_FLOW | JST |
| MUSCL_FLOW | YES |
| SLOPE_LIMITER_FLOW | VENKATAKRISHNAN |
| VENKAT_LIMITER_COEFF | 0.03 |
| JST_SENSOR_COEFF | ( 0.5, 0.02 ) |
| TIME_DISCRE_FLOW | EULER_IMPLICIT |
| KIND_TURB_MODEL | SA |
| PRANDTL_TURB | 0.90 |
| CONV_NUM_METHOD_TURB | SCALAR_UPWIND |
| MUSCL_TURB | NO |
| SLOPE_LIMITER_TURB | VENKATAKRISHNAN |
| TIME_DISCRE_TURB | EULER_IMPLICIT |

Two guidelines were used to determine convergence of simulations. First, the square root of the sum of squares of the residuals of all conservation variables should be constant or steadily decreasing. Second, the results of interest should be unchanging over a large number of iterations. The results of interest are the plots shown in this paper. All simulations were run to at least 300,000 iterations and intermediate checks were performed about every 50,000 iterations. All residuals steadily decreased between 100,000 and 350,000 iterations. Final residual values are on the order of $10^{-7}$ for clean-missile simulations and $10^{-6}$ for missile-fin simulations. All clean-missile plots were checked to be identical at the presented scales at 200,000 and 300,000 iterations. All missile-fin plots were checked to be identical at 250,000, 300,000, and 350,000 iterations at the presented scales. The 300,000 iteration results were used for figures.

The Python function written to perform the Rayleigh Pitot formula calculation is reproduced here:

```
def pitot_formula(P1,M1):
   #Returns P02 given P1 and M1
   gamma = 1.4
   P2_P1 = (2*gamma*M1**2-(gamma-1))/(gamma+1)
   M2_squared = ((gamma-1)*M1**2+2)/(2*gamma*M1**2-(gamma-1))
   P02_P2 = (1+((gamma-1)/2)*(M2_squared))**(gamma/(gamma-1))
   return P02_P2*P2_P1*P1
```

## Acknowledgments

This work was supported by AFRL under contract FA8650-18-C-2253 (program manager J. Boston). The material in this paper was assigned a clearance of CLEARED (case number 88ABW-2019-5338). Computational resources were provided by the AFRL DSRC and by Information Technology at Purdue University, West Lafayette, Indiana.

## References

[1] Smith, D., Petley, D., Edwards, C., and Patten, A., "An investigation of gap heating due to stepped tiles in zero pressure gradient regions of the Shuttle Orbiter Thermal Protection System," AIAA Paper 1983-120. doi: 10.2514/6.1983-120

[2] Dolling, D. S., "Fifty Years of Shock-Wave/Boundary-Layer Interaction Research: What Next?," *AIAA Journal*, Vol. 39, Aug. 2001, pp. 1517-1531. doi: 10.2514/2.1476

[3] Law, C. H., "Three-Dimensional Shock Wave-Turbulent Boundary Layer Interactions at Mach 6," Aerodynamics Research Laboratory (ARL) Interim Report AD-A014 738, Jun. 1975. doi: 10.21236/ada014738

[4] Neumann, R. D., and Hayes, J. R., "Aerodynamic Heating In The Fin Interaction Region Of Generalized Missile Shapes At Mach 6," AFFDL-TR-79-3066, May 1979.

[5] Economon, T. D., Palacios, F., Copeland, S. R., Lukaczyk, T. W., and Alonso, J. J., "SU2: An Open-Source Suite for Multiphysics Simulation and Design," *AIAA Journal*, Vol. 54, Mar. 2016, pp. 828-846. doi: 10.2514/1.J053813

[6] Pointwise, Ver. 18.3 Release 1, Pointwise Inc., Fort Worth, TX.

[7] Spalart, P., and Allmaras, S., "A one-equation turbulence model for aerodynamic flows," AIAA Paper 1992-439, Jun. 1992. doi: 10.2514/6.1992-439

[8] Prandtl, L, "Bericht uber Untersuchungen zur ausgebildeten Turbulenz," *Zeitschrift fur angewndte Mathematik und Mechanik*, Vol. 5 no. 2, April 1925, pp. 136-139.

[9] Ali, Z., and Tucker, P. G., "Multiblock Structured Mesh Generation for Turbomachinery Flows," *Proceedings of the 22nd International Meshing Roundtable*, 2014, pp. 165–182. doi: 10.1007/978-3-319-02335-9_10

[10] Sorenson, R.L., The 3DGRAPE Book: Theory, Users' Manual, Examples, NASA TM-102224, July 1989.

[11] Tecplot 360, Ver. EX 2017 R3, Tecplot Inc., Bellevue, WA.

[12] Python, Ver. 2.7, Python Software Foundation, Wilmington, DE.

[13] Oliphant, T, "A guide to NumPy," USA: Trelgol Publishing, 2006.

[14] Hunter, J.D., "Matplotlib: A 2D Graphics Environment," *Computing in Science & Engineering*, Vol. 9 no. 3, 2007, pp. 90-95.